THERMOELECTRIC PERFORMANCE OF Fe_2ALV/CNT-BASED ALLOYS

by

Emad M. ELSEHLY[a,b*], Adel Bandar ALRUQI[c*], Abdelmoneim EL-KHOULY[a,b], Vlademir KHOVAYLO[b], Haifa S. ALQANNAS[d], Ahmed HAKAMY[e], Wael M. F. ABDEL-REHIM[f,g], and Alaa M. ADAM[g,h]

[a]Physics Department, Faculty of Science, Damanhour University, Damanhour, Egypt
[b]National University of Science and Technology MISIS, Moscow, Russian Federation
[c]Department of Physics, Faculty of Science, King Abdulaziz University, Jeddah, Saudi Arabia
[d]Department of Physics, Faculty of Science, University of Jeddah, Jeddah, Saudi Arabia
[e]Department of Physics, Faculty of Applied Science, Umm Al-Qura University, Makkah, Saudi Arabia
[f]Faculty of Computers and Information, Suez University, Suez, Egypt
[g]Faculty of Engineering, King Salman International University, South Sinai, Egypt
[h]Physics Department, Faculty of Science, Sohag University, Sohag, Egyp

Original scientific paper
https://doi.org/10.2298/TSCI221005194E

Heusler-type $Fe_2AlV_xTi_{1-x}$ alloys offer an alternative solution for the generation of thermoelectric power near room temperature. In the current research, thermoelectric properties of the p-type $Fe_2AlV_{0.9}Ti_{0.1}$ and $Fe_2AlV_{0.9}Ti_{0.1}$/CNT alloys, prepared by SPS, were studied. Carbon nanotubes (CNT) were used as dopants to improve the seebeck coefficient and electrical conductivity. Upon doping with CNT, the thermal conductivity was significantly reduced, meanwhile, the value of the power factor increased from 0.45 to 1.55 mW/mK^2 at around 330 K. The effect of CNT inclusions on the thermoelectric parameters of $Fe_2AlV_xTi_{1-x}$ compounds was systematically studied. When compared to $Fe_2AlV_{0.9}Ti_{0.1}$, which had a figure of merit of just 0.02 at 330 K, the CNT-containing samples showed a significantly improved figure of merit up to 0.07. We offer a novel technique to improve the performance of Fe_2AlV alloys.

Key words: *Fe_2AlV alloy, electrical properties, thermoelectric materials, heusler alloy, carbon nanotubes.*

Introduction

Thermoelectric technology, which is based on the Peltier and Seebeck phenomena, enables the direct conversion of heat into electricity, providing a sustainable energy conversion option [1]. The most important aspect determining this technology's ability to convert energy efficiently is its dimensionless figure of merit ZT for thermoelectric materials. The ZT is commonly expressed using the following relation:

$$ZT = \frac{S^2\sigma}{k}T \tag{1}$$

*Corresponding authors, e-mail: elsehlyfigo@yahoo.com, aalruqi@ksu.edu.sa

where the parameters of this equation were defined in [2]. Over the past few decades, numerous efforts have been undertaken to improve the thermoelectric capability of different materials using several techniques, such as doping engineering [3]. Because their constituent parts are readily available, inexpensive, and have strong thermoelectric capabilities, Heusler compounds based on iron fully satisfy the demands of industrial waste heat harvest technologies. These intermetallic complexes, however, continue to be fragile and call for processing techniques. [4].

A promising material to produce thermoelectric power near the room temperature is Fe_2AlV Heusler alloy. In the Fe_2AlV system, the doping elements, for example the Si substitution for Al site in the *n*-type and Ti instead of V in *p*-type, can be used to simultaneously increase the power factor and control the type of conduction [5, 6]. Owing to their thermal conductivity that could reach ~28 W/mK, the Fe_2AlV alloys have low ZT values [7]. As a result, and compared to modern thermoelectric materials, its efficiency of thermoelectric energy conversion is significantly smaller. Therefore, reduction of κ is required for functional applications [8]. The fabrication of composites based on a thermoelectric matrix and a nano-dispersed filler is one of the effective methods for enhancing the thermoelectric ZT of materials. It is feasible to significantly lower the lattice thermal conductivity by boosting the scattering of medium- and long-wavelength phonons at the interfaces between the matrix and the filler [9].

Due to its superior mechanical properties, extreme mobility of the charge carrier, and small band gap energy, CNT is one of the possible interesting TE materials. Furthermore, CNT are a suitable inclusion material for thermoelectric materials since they are commercially available in large quantities and exhibit little to no impact on the environment and eco systems [10]. Many structural and functional materials use CNT as additions to enhance their qualities [10]. Despite having modest thermoelectric characteristics, CNT exhibit strong heat conductivity and a low seebeck coefficient, they are frequently added to various thermoelectric materials [11]. The CNT impact on the thermoelectric characteristics of materials based on Bi_2Te_3 was a topic of active research [12, 13]. Additionally, research on the effects of CNT on the thermoelectrical properties of various chemicals and polymers were described in the literature [14, 15]. As known, the CNT doping effect related to the characteristics of Heusler alloys was not yet studied. Considering the growing interest in studying the CNT effects on the thermoelectrical properties of compounds [16], we present a systematic study on selected materials based on *p*-type Heusler alloys of Fe_2AlV system and added CNT to the alloys. In the current study, we investigate the effect of CNT doping on the thermoelectric properties of $Fe_2AlV_{0.9}Ti_{0.1}$ alloys.

Experimental methods

Crystalline alloys of nominal chemical composition of *p*-type $Fe_2AlV_{0.9}Ti_{0.1}$ were synthesized from initial chemical elements of high purity (99.999%) by arc and induction melting in argon atmosphere. To enhance the homogeneity of the samples, the ingots in the arc furnace were remelted three times. At a high temperature of 1073 K, the prepared samples were annealed for 72 hours in evacuated quartz tubes and then the annealed alloys were quenched in cold water. The ingots that subjected to annealing were crushed to a fine powder and divided into two components. Commercial powder of multiwalled CNT (Taunit-M) with (5 μm in length, 15-25 nm in average outer diameter, and 234 m^2/g specific surface area) were purified as reported in [17]. The CNT were added to the powder of the as prepared ingots in an amount of 2% by weight.

The CNT were mixed to the powder of the prepared alloy in a ball mill with a 450 rpm rotation speed using a ratio of balls to powder mixture of 10:1 in argon atmosphere for 4 hours. On a spark plasma sintering (SPS) unit Labox 650, Sinter Land, the powders were mixed under a vacuum at a pressure of 50 MPa, and temperatures of 1023 K, the detailed process in the SPS unit is described in [18]. Circular disk-shaped synthetic samples were annealed for two days at 1073 K. The phase composition of the concerned samples was analyzed on a Difrey 401 diffractometer using CrKα (λ = 2.2909 Å) radiation. For qualitative elemental analysis, a Tescan SEM with energy dispersive analysis was used. From the thermal diffusivity measured using the laser flash method on a Netzsch LFA 447 unit in the temperature range of 300-473 K, the thermal conductivity of the alloys was estimated. Utilizing the four-probe approach and differential techniques, respectively, the temperature dependences of electrical conductivity and thermoelectric EMF coefficient were evaluated within the temperature range of 300-473 K.

Results and discussions

Samples characterization

The XRD measurements were performed on sintered $Fe_2AlV_{0.9}Ti_{0.1}$ (FVA) and $Fe_2AlV_{0.9}Ti_{0.1}$/CNT (FVA-CNT) alloys to examine the crystal structure and identify the different phases that comprise the obtained samples. As can be seen in fig. 1, the Fe_2AlV Heusler-type (L21) structure was recognized for all the diffraction peaks from each sample. The XRD results for the FVA-CNT samples did not indicate any impurity phases. The positions of the main peaks correspond to the cubic structure with the lattice parameter a = 3.49093 Å for FVA and a = 3.48816 Å for FVA-CNT, respectively, see tab. 1 which is strongly consistent with the evidence from the [19]. The narrow and sharp peaks in the X-ray patterns reveal the high crystallization of the samples under investigation. Crystallite size (D) is presented in tab. 1. This was calculated using Scherrer's equation from XRD patterns:

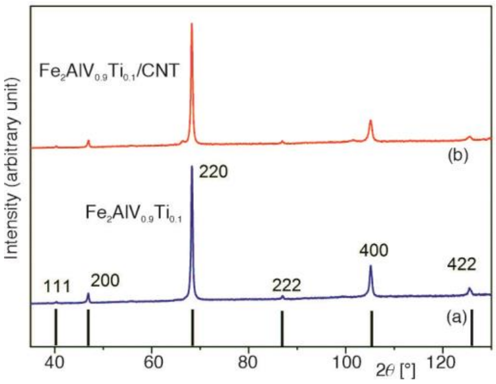

Figure 1. The patterns of XRD diffracted from the sintered alloys; (a) the $Fe_2AlV_{0.9}Ti_{0.1}$ and (b) the $Fe_2AlV_{0.9}Ti_{0.1}$/CNT

$$D = \frac{K\lambda}{\beta\cos\theta} \tag{2}$$

As K = 0.9 correlated to the crystallite shape, λ is the X-ray wavelength, β is the full width at half maximum (FWHM) in radians, and the Bragg angle is θ. The D values increased notably after CNT doping, as shown in tab. 1. This increase in grain size may be due to the lattice strain following CNT doping [20].

Table 1. Crystallite size, the lattice parameter, and the experimental density of the $Fe_2AlV_{0.9}Ti_{0.1}$, and $Fe_2AlV_{0.9}Ti_{0.1}$/CNT alloys

Sample	D [nm]	a [Å]	Density [gmcm^{-3}]
$Fe_2AlV_{0.9}Ti_{0.1}$	72.2567	3.49093	6.4112
$Fe_2AlV_{0.9}Ti_{0.1}$/CNT	135.506	3.48816	6.3714

After SPS treatment, the samples' microstructure and surface morphology were determined using the SEM analysis. The SEM micrographs are present in fig. 2. The SEM images of the FVA and FVA-CNT samples revealed higher densification of the alloys, as no obvious cracks or voids. The rise in grain size following CNT doping is significant. Table 2 represents the experimental density of the $Fe_2AlV_{0.9}Ti_{0.1}$ and $Fe_2AlV_{0.9}Ti_{0.1}$/CNT alloys. The density of the CNT samples shows a relatively small density, this due to the lower density of CNT [21].

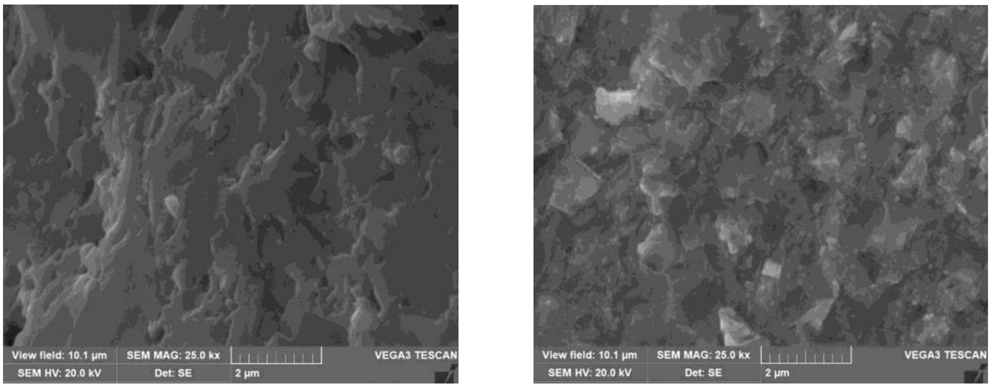

Figure 2. The SEM micro images of $Fe_2AlV_{0.9}Ti_{0.1}$ system (left) and $Fe_2AlV_{0.9}Ti_{0.1}$/CNT (right)

Quantitative analysis of composition constituents, in terms of the percentage of all elements present in each sample was conducted by the energy X-ray spectroscopy (EDX). The actual elemental percentage, with different atomic ratios, is in good agreement with the corresponding nominal levels, according to EDX data, fig. 3, and tab. 2.

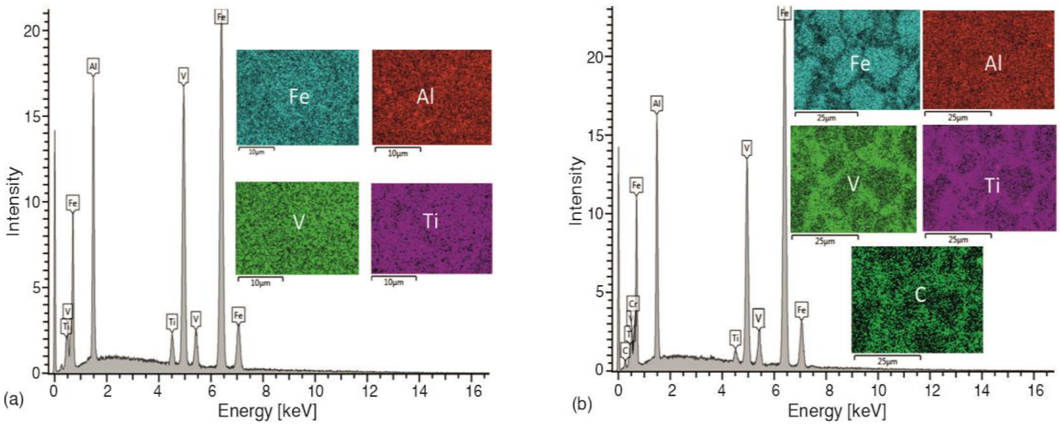

Figure 3. The EDAX spectra of $Fe_2AlV_{0.9}Ti_{0.1}$ system (a) and $Fe_2AlV_{0.9}Ti_{0.1}$/CNT (b)

Table 2. Elemental distribution given by EDX analysis

Sample	Fe [%]	Al [%]	V [%]	Ti [%]	C [%]
$Fe_2AlV_{0.9}Ti_{0.1}$	50.2	25.1	22.3	2.4	–
$Fe_2AlV_{0.9}Ti_{0.1}$/CNT	50.8	24	18.1	1.7	5.4

Thermoelectric parameters

Electrical conductivity and the seebeck coefficient as functions of temperature

The thermoelectric parameters, seebeck coefficient, *S*, and the electrical conductivity, σ, within the range of temperature from 320 K to 465 K for the samples $Fe_2AlV_{0.9}Ti_{0.1}$, and $Fe_2AlV_{0.9}Ti_{0.1}$/CNT are presented in figs. 4(a) and 4(b). The achieved results show that the CNT doping strongly affected the thermoelectric properties of Heusler alloys. Figure 4(a) shows remarkable increase in the value of σ as the temperature increase for both samples. The $Fe_2AlV_{0.9}Ti_{0.1}$/CNT samples showed higher σ than the alloy without CNT. The FVA-CNT had an electrical conductivity maximum of $340 \times 10^3\ \Omega^{-1}m^{-1}$ at 465 K., while a value of $195 \times 10^3\ \Omega^{-1}m^{-1}$ for the FVA sample, fig. 4(a). The enhancement in the electrical conductivity for FVA-CNT alloys strongly contributes to increased thermoelectric efficiency.

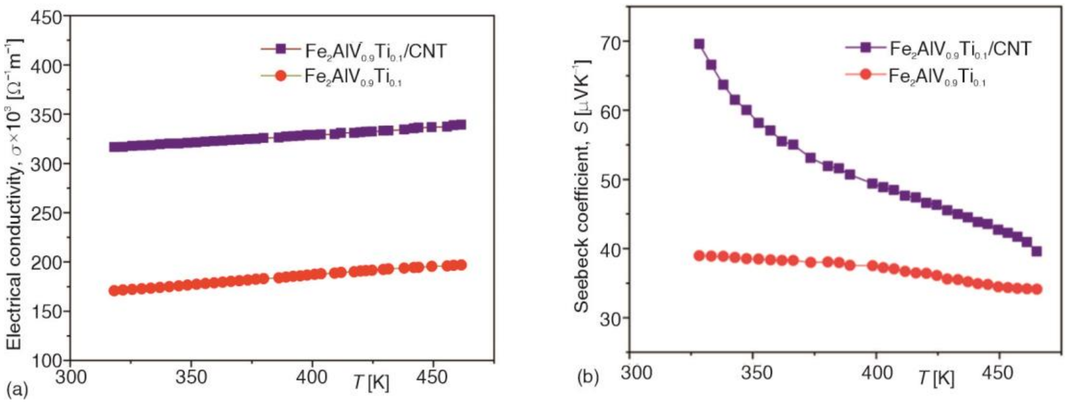

Figure 4. The electrical conductivity (a) and seebeck coefficient (b) *vs.* temperature for $Fe_2AlV_{0.9}Ti_{0.1}$ and $Fe_2AlV_{0.9}Ti_{0.1}$/CNT samples

Figure 4(b) shows the seebeck coefficient variation of the two samples within the temperature range. The *p*-type conduction was discovered in the systems in consideration, as shown by the positive sign of the seebeck coefficient. As clearly seen, seebeck coefficient decreases with increasing the measuring temperature. Adding CNT to FVA system is accompanied by an enhancement in the values of seebeck coefficient by almost one order of magnitude. The $Fe_2AlV_{0.9}Ti_{0.1}$/CNT had a maximum seebeck coefficient of 70 μVK^{-1} at ~315 K, that is higher compared to the FVA sample.

The significant effects upon the adding of CNT on the properties of the thermoelectric FVA Heusler alloys, fig. 4, can be qualitatively explained considering the type of conductivity of the CNT themselves [22-25]. Taking into account that CNT are *p*-type conductors with the seebeck coefficient at room temperature ~20-40 μVK^{-1} [26-28], their addition to the Heusler alloy $Fe_2AlV_{0.9}Ti_{0.1}$ which is *p*-type, leads to a relatively high change in both seebeck coefficient and σ, fig. 4. Clearly, doping and alloying is quite effective strategy for enhancing the materials thermoelectric performance [29-31].

The power factor and the thermal conductivity as a function of temperature

The power factor, PF = $S2\sigma$ is another variable that fits the behavior of the seebeck coefficient. It is evident that when temperatures rise, the power factor falls, as shown in fig.

5(a). Additionally, within the investigated temperature range, the CNT doped samples exhibit an improvement in the power factor compared to the un-doped ones. With a value of 1.6 $mWm^{-1}K^{-2}$ at 325 K, the $Fe_2AlV_{0.9}Ti_{0.1}$/CNT alloy had the highest power factor. Although p-type $Fe_2AlV_{0.9}Ti_{0.1}$/CNT sample have the largest power factor, however, has lower thermal conductivity compared with $Fe_2AlV_{0.9}Ti_{0.1}$ samples, fig. 5(b). Data on the thermal conductivity, k, of the relevant samples, both with and without the addition of carbon nanotubes, support this supposition.

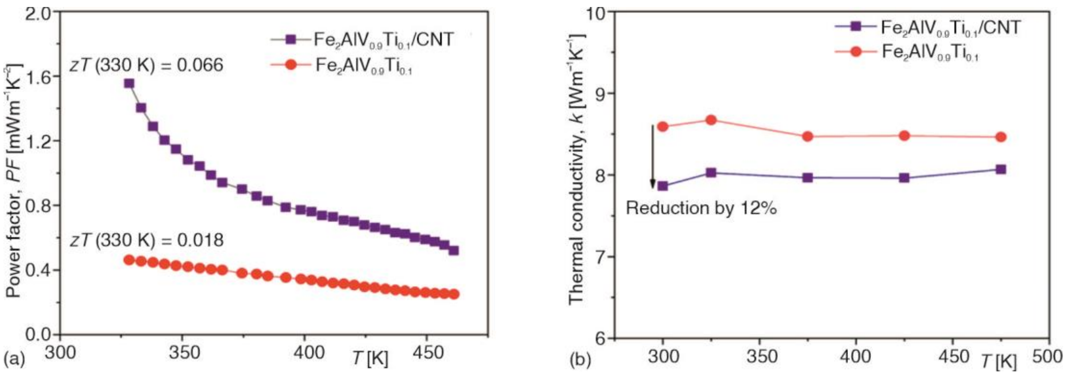

Figure 5. The power factor (a) and the total thermal conductivity (b) as a function of temperature for the samples $Fe_2AlV_{0.9}Ti_{0.1}$ and $Fe_2AlV_{0.9}Ti_{0.1}$/CNT

Figure 5(b) shows that the inclusion of CNT significantly reduces the thermal conductivity of $Fe_2AlV_{0.9}Ti_{0.1}$, which is probably due to phonon scattering mechanisms at the interfaces between the nanotubes and matrix. The thermal conductivity of $Fe_2AlV_{0.9}Ti_{0.1}$ significantly decreased at room temperature by a factor of 12%.

The figure of merit (Q-factor)

The behaviour of zT of, as a function of temperature, is shown in fig. 6. Figure 6 illustrates the behavior of zT of $Fe_2AlV_{0.9}Ti_{0.1}$ and $Fe_2AlV_{0.9}Ti_{0.1}$/CNT as a function of temperature. As clearly indicated, the samples with CNT doping have the highest zT. Consequently, the FVA-CNT sample at 320 K figure of merit zT increased by almost 250%, from 0.02 for FVA to 0.07. Because it has the highest seebeck coefficient and largest power factor, the $Fe_2AlV_{0.9}Ti_{0.1}$/CNT sample has the highest zT. Due to the lower thermal conductivity and higher power factor, we were able to produce an alloy based on Fe_2VAl/CNT that had higher zT values than the pristine bulk alloy. Although we obtained a zT value of 0.07 in the current study which is relatively small, we have the opportunity to improve it by the optimization of the CNT parameters.

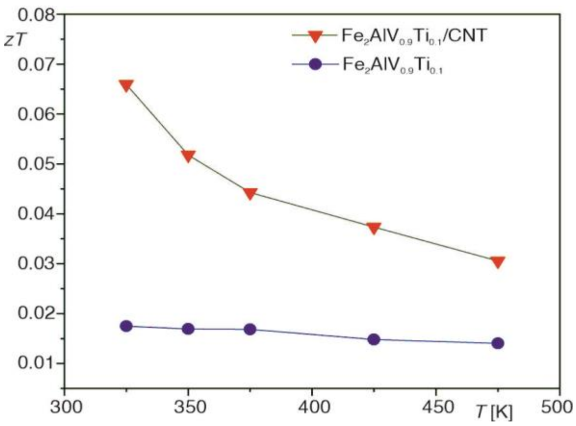

Figure 6. The Q-factor (zT) as a function of temperature for the alloys $Fe_2AlV_{0.9}Ti_{0.1}$ and $Fe_2AlV_{0.9}Ti_{0.1}$/CNT

Conclusion

The research presents a novel investigation of the impact of CNT on the thermoelectric properties of *p*-type $Fe_2AlV_{0.9}Ti_{0.1}$ Heusler alloys. It was revealed that CNT addition improved the electrical conductivity and thermoelectric power. The $Fe_2AlV_{0.9}Ti_{0.1}$/CNT showed a reduced thermal conductivity. The improvement in the figure of merit is caused by the decrease in thermal conductivity and the rise in power factor. At room temperature, the $Fe_2AlV_{0.9}Ti_{0.1}$/CNT alloys' figure of merit zT achieved 0.07. Following these results in the future, it looks interesting to study the efficiency of the thermoelectric materials with different CNT content, which will make it possible to determine the percolation threshold and optimizing the thermoelectric properties of Heusler compounds with CNT content. We anticipate that the great endurance of the Heusler alloy and the low cost of the CNT element will be advantageous in practical systems.

Acknowledgment

The authors would like to thank the Deanship of Scientific Research at Umm Al-Qura University for supporting this work by Grant Code (22UQU4250045DSR18)

References

[1] Adam, A. M., *et al*., Preparation and Thermoelectric Power Properties of Highly Doped p-Type Sb_2T_{e3} Thin Films, *Physica E: Low-Dimensional Systems and Nanostructures*, *127* (2021), 114505
[2] Adam, A. M., *et al*., Thermoelectric Power Properties of Ge Doped PbTe Alloys, *Journal of Alloys and Compounds, 872* (2021), 159630
[3] Pei, Y, *et al*., Convergence of Electronic Bands for High Performance Bulk Thermoelectric, *Nature, 473* (2011), May, pp. 66-69
[4] El-Khouly, A., *et al*. Mechanical and Thermoelectric Properties of FeVSb-Based Half-Heusler Alloys, *Journal of Alloys and Compounds, 886* (2021), 161308
[5] Hitoshi, M., *et al*., Doping Effects on Thermoelectric Properties of the Pseudogap Fe2VAl System, *Journal of the Japan Institute of Metals and Materials, 66* (2002), 7, pp. 767-771
[6] Masashi, M., *et al*., Power Generation Performance of Thermoelectric Module Consisting of Sb-Doped Heusler Fe2VAl Sintered Alloy, *Materials Transactions, 52* (2011), 8, pp. 1546-1548
[7] Alleno, E., Review of the Thermoelectric Properties in Nanostructured Fe2Val, *Metals, 8* (2018), 11, 864
[8] Mikami, M., *et al*.,Synthesis and Thermoelectric Properties of Microstructural Heusler Fe2VAl Alloy, *Journal of Alloys and Compounds, 461* (2008), 0925-8388
[9] Ruiheng, L., *et al*., Low Thermal Conductivity and Enhanced Thermoelectric Performance of Gd-Filled Skutterudites, *Journal of Applied Physics, 109* (2011), 023719
[10] Yizeng, W., *et al*., Application-Driven Carbon Nanotube Functional Materials, *ACS Nano, 15* (2021), 5, pp. 7946-7974
[11] Hung, N. T., *et al*., Thermoelectric Properties of Carbon Nanotubes, *Energies, 12* (2019), 23, 4561
[12] Zhang, Y., *et al*., Publisher's Note: Electrical and Thermoelectric Properties of Single-Wall Carbon Nanotube Doped Bi_2Te_3, *Appl. Phys. Lett., 101* (2012), 031909, *Appl. Phys. Lett., 102* (2013), 019902
[13] Bartosz, T. *et al*., Structure and Thermoelectric Properties of Bismuth Telluride – Carbon Composites, *Materials Research Bulletin, 99* (2018), Mar., pp.10-17
[14] Ge, N., *et al*., High Performance Thermoelectric Module Through Isotype Bulk Heterojunction Engineering of Skutterudite Materials, *Nano Energy, 66* (2019), 104193
[15] Jueshuo, F., *et al*., Feasibility of Using Chemically Exfoliated Snse Nanobelts in Constructing Flexible Swcnts-Based Composite Films for High-Performance Thermoelectric Applications, *Composites Communications*, *24* (2021), 100612
[16] Yusupov, K., Vomiero, A., Polymer-Based Low-Temperature Thermoelectric Composites, *Adv. Funct. Mater., 30* (2020), 2002015
[17] Elsehly, E. M., *et al*., Ozone Functionalized CNT-Based Filters for High Removal Efficiency of Benzene from Aqueous Solutions, *J. Water Process Eng., 25* (2018), Oct., pp. 81-87

[18] Osvenskiy, V. B., *et al*., Nonmonotonic Change in the Structural Grain Size of the $Bi_{0.4}Sb_{1.6}Te_3$ Thermoelectric Material Synthesised by Spark Plasma Sintering, *J. Alloys Compd., 586* (2014), Suppl. 1, S413-S418
[19] Nishino, Y., Tamada, Y., Doping Effects on Thermoelectric Properties of the Off-Stoichiometric Heusler Compounds Fe_2–xV_1+xAl, *Journal of Applied Physics, 115* (2014), 123707
[20] Porter, D. A., *et al*., *Phase Transformations in Metals and Alloys (Revised Reprint)*, CRC Press, Boca Raton, Fla., USA, 2009
[21] Elsehly, E M., *et al*., Morphological and Structural Modifications of Multiwalled Carbon Nanotubes by Electron Beam Irradiation, *Mater. Res. Express, 3* (2016), 105013
[22] Popov, V. N., Carbon Nanotubes: Properties and Application, *Materials Science and Engineering: R: Reports, 43* (2004), 3, pp. 61-102
[23] Hung, T., *et al*., Thermoelectric Properties of Carbon Nanotubes, *Energies, 12* (2019), 23, 4561
[24] Park, D. H., *et al*., Thermoelectric Energy-Conversion Characteristics of n-Type $Bi_2(Te, Se)_3$ Nanocomposites Processed with Carbon Nanotube Dispersion, *Curr. Appl. Phys., 11* (2011), 4, pp. S41-S45
[25] Elsehly, E. M., *et al*., Annealing Effect on the Thermoelectric Properties of Multiwall Carbon Nanotubes, *Physica E: Low-Dimensional Systems and Nanostructures, 146* (2023), 115566
[26] Zhang, Y., *et al*., Electrical and Thermoelectric Properties of Single-Wall Carbon Nanotube Doped Bi_2Te_3, *Appl. Phys. Lett. 101* (2012), 031909
[27] Ren, F., *et al*., Thermoelectric and Mechanical Properties of Multi-Walled Carbon Nanotube Doped $Bi_{0.4}Sb_{1.6}Te_3$ Thermoelectric Material, *Appl Phys Lett, 103* (2013), 221907
[28] Bark, H., *et al*., Effect of Multiwalled Carbon Nanotubes on the Thermoelectric Properties of a Bismuth Telluride Matrix, *Current Applied Physics, 13* (2013), Suppl. 2, pp. S111-S114
[29] Adam, A. M., *et al*., Optimized Thermoelectric Performance in Thin $(Bi_2Se_3)_{1-x}(Bi_2Te_3)_x$ Alloyed Films, *Journal of Alloys and Compounds, 898* (2022) 162888
[30] El-Khouly, A., *et al*., Transport and Thermoelectric Properties of Nb-Doped $FeV_{0.64}Hf_{0.16}Ti_{0.2}Sb$ Half-Heusler Alloys Synthesized by Two Ball Milling Regimes, *Journal of Alloys and Compounds, 890* (2022), 161838
[31] El-Khouly, A., *et al*., Optimizing the Thermoelectric Performance of FeVSb Half-Heusler Compound via Hf–Ti Double Doping, *Journal of Power Sources, 477* (2020) 228768

Paper submitted: October 5, 2022
Paper revised: November 7, 2022
Paper accepted: November 23, 2022